Modeling the specular spectral reflectance of partially ordered alumina nanopores on an aluminum substrate

Dengfeng Kuang,[1,2,*] Renée Charrière,[3] Natalia Matsapey,[3] Manuel Flury,[4] Jenny Faucheu,[3] and Pierre Chavel[1,5]

[1]*Laboratoire Hubert Curien, Université Jean-Monnet de Saint-Etienne, CNRS et Institut d'Optique Graduate School, 18, rue du Professeur Benoît Lauras, 42000 Saint-Etienne, France*
[2]*Key Laboratory of Optical Information Science and Technology (Ministry of Education), Institute of Modern Optics, Nankai University, Tianjin 300071, China*
[3]*Ecole Nationale Supérieure des Mines de Saint-Etienne, SMS EMSE, CNRS: UMR5307, LGF: Laboratoire Georges Friedel, 158 cours Fauriel, 42023 Saint-Etienne, France*
[4]*Laboratoire ICube, CNRS: UMR7357, 300 boulevard Sébastien Brant, 67412 Illkirch, France*
[5]*Laboratoire Charles Fabry, Institut d'Optique, CNRS, Univ. Paris Sud, 2, avenue Augustin Fresnel, 91127 Palaiseau, France*
[*]*dfkuang@nankai.edu.cn*

Abstract: Anodizing of aluminum generates a porous alumina layer comprising cylindrical nanopores (300 nm diameter) extending essentially perpendicular to the substrate. The pore distribution over the surface exhibits a short-distance order close to hexagonal arrangement. On the contrary, long-distance order cannot be defined: the arrangement is not periodic. Visual observation of such nanoporous layers shows a reddish specular reflectance consistent with reflectance spectrum measurements. This work is a parametric study aiming at demonstrating that color effects are caused by the presence of disorder illustrated by the deviations from periodicity in terms of nanopore location and nanopore radius. Using the method of Rigorous Coupled Wave Analysis (RCWA), the reflectance spectrum has been simulated. Although our calculations were done using a simple one-dimensional (1D) model, a fair fit with experimental results is found.

OCIS codes: (310.6628) Subwavelength structures, nanostructures; (260.2110) Electromagnetic optics; (290.1483) BSDF, BRDF, and BTDF; (310.6188) Spectral properties.

References and links

1. A. Oskooi, P. A. Favuzzi, Y. Tanaka, H. Shigeta, Y. Kawakami, and S. Noda, "Partially disordered photonic-crystal thin films for enhanced and robust photovoltaics," Appl. Phys. Lett. **100**(18), 181110 (2012).
2. K. Vynck, M. Burresi, F. Riboli, and D. S. Wiersma, "Photon management in two-dimensional disordered media," Nat. Mater. **11**(12), 1017–1022 (2012).
3. C. Bauer, G. Kobiela, and H. Giessen, "2D quasiperiodic plasmonic crystals," Sci Rep **2**, 681 (2012).
4. F. Przybilla, C. Genet, and T. W. Ebbesen, "Enhanced transmission through penrose subwavelength hole arrays," Appl. Phys. Lett. **89**(12), 1211151 (2006).
5. T. Matsui, A. Agrawal, A. Nahata, and Z. V. Vardeny, "Transmission resonances through aperiodic arrays of subwavelength apertures," Nature **446**(7135), 517–521 (2007).
6. C. Rockstuhl, F. Lederer, T. Zentgraf, and H. Giessen, "Enhanced transmission of periodic, quasiperiodic, and random nanoaperture arrays," Appl. Phys. Lett. **91**(15), 151109 (2007).
7. T. Schwartz, G. Bartal, S. Fishman, and M. Segev, "Transport and Anderson localization in disordered two-dimensional photonic lattices," Nature **446**(7131), 52–55 (2007).
8. L. Levi, M. Rechtsman, B. Freedman, T. Schwartz, O. Manela, and M. Segev, "Disorder-enhanced transport in photonic quasicrystals," Science **332**(6037), 1541–1544 (2011).
9. D. Molinari and A. Fratalocchi, "Route to strong localization of light: the role of disorder," Opt. Express **20**(16), 18156–18164 (2012).
10. S. Mazoyer, J. P. Hugonin, and P. Lalanne, "Disorder-induced multiple scattering in photonic-crystal waveguides," Phys. Rev. Lett. **103**(6), 063903 (2009).

#228505 - $15.00 USD Received 24 Nov 2014; revised 19 Jan 2015; accepted 29 Jan 2015; published 12 Feb 2015

11. S. Mazoyer, P. Lalanne, J. C. Rodier, J. P. Hugonin, M. Spasenović, L. Kuipers, D. M. Beggs, and T. F. Krauss, "Statistical fluctuations of transmission in slow light photonic-crystal waveguides," Opt. Express **18**(14), 14654–14663 (2010).
12. J. P. Vigneron, V. Lousse, L. P. Biró, Z. Vértesy, and Z. Bálint, "Reflectance of topologically disordered photonic-crystal films," Proc. SPIE **5733**, 308–315 (2005).
13. D. G. Stavenga, J. Tinbergen, H. L. Leertouwer, and B. D. Wilts, "Kingfisher feathers--colouration by pigments, spongy nanostructures and thin films," J. Exp. Biol. **214**(23), 3960–3967 (2011).
14. H. Noh, S. F. Liew, V. Saranathan, S. G. Mochrie, R. O. Prum, E. R. Dufresne, and H. Cao, "How noniridescent colors are generated by quasi-ordered structures of bird feathers," Adv. Mater. **22**(26-27), 2871–2880 (2010).
15. A. E. Seago, P. Brady, J.-P. Vigneron, and T. D. Schultz, "Gold bugs and beyond: a review of iridescence and structural colour mechanisms in beetles (Coleoptera)," J. R. Soc. Interface **6**(Suppl 2), S165–S184 (2009).
16. C. Pouya, D. G. Stavenga, and P. Vukusic, "Discovery of ordered and quasi-ordered photonic crystal structures in the scales of the beetle Eupholus magnificus," Opt. Express **19**(12), 11355–11364 (2011).
17. J. W. Diggle, T. C. Downie, and C. W. Goulding, "Anodic oxide films on aluminum," Chem. Rev. **69**(3), 365–405 (1969).
18. Q. Xu, H. Y. Sun, Y. H. Yang, L. H. Liu, and Z. Y. Li, "Optical properties and color generation mechanism of porous anodic alumina films," Appl. Surf. Sci. **258**(5), 1826–1830 (2011).
19. X. H. Wang, T. Akahane, H. Orikasa, T. Kyotani, and Y. Y. Fu, "Brilliant and tunable color of carbon-coated thin anodic aluminum oxide films," Appl. Phys. Lett. **91**(1), 011908 (2007).
20. X. L. Zhao, G. W. Meng, Q. L. Xu, F. M. Han, and Q. Huang, "Color fine-tuning of CNTs@AAO composite thin films via isotropically etching porous AAO before CNT growth and color modification by water infusion," Adv. Mater. **22**(24), 2637–2641 (2010).
21. X. Wang, D. Zhang, H. Zhang, Y. Ma, and J. Z. Jiang, "Tuning color by pore depth of metal-coated porous alumina," Nanotechnology **22**(30), 305306 (2011).
22. C. Y. Yang, W. D. Shen, Y. G. Zhang, Z. J. Ye, X. Zhang, K. Li, X. Fang, and X. Liu, "Color-tuning method by filling porous alumina membrane using atomic layer deposition based on metal-dielectric-metal structure," Appl. Opt. **53**(4), A142–A147 (2014).
23. I. Maksymov, J. Ferré-Borrull, J. Pallarès, and L. F. Marsal, "Photonic stop bands in quasi-random nanoporous anodic alumina structures," Photonics and Nanostructures: Fundamentals and Applications **10**, 459–462 (2012).
24. M. G. Moharam, E. B. Grann, D. A. Pommet, and T. K. Gaylord, "Formulation for stable and efficient implementation of the rigorous coupled-wave analysis of binary gratings," J. Opt. Soc. Am. A **12**(5), 1068–1076 (1995).
25. P. Lalanne and G. M. Morris, "Highly improved convergence of the coupled-wave method for TM polarization," J. Opt. Soc. Am. A **13**(4), 779–784 (1996).
26. J. P. Hugonin and P. Lalanne, Reticolo software for grating analysis, see *www.lp2n.institutoptique.fr*
27. N. Matsapey, "Rendu visual de surfaces nanostructurées: effet de l'ordre à courte distance," thèse de doctorat en sciences, École Nationale Supérieure des Mines de Saint-Étienne (2013).
28. N. Matsapey, J. Faucheu, M. Flury, and D. Delafosse, "Design of a gonio-spectro-photometer for optical characterization of gonio-apparent materials," Meas. Sci. Technol. **24**(6), 065901 (2013).
29. J. C. Maxwell-Garnett, "Colours in metal glasses and in metallic films," Philos. Trans. R. Soc. London, Sect. A **3**, 385–420 (1904).
30. A. D. Rakic, A. B. Djurišic, J. M. Elazar, and M. L. Majewski, "Optical properties of metallic films for vertical-cavity optoelectronic devices," Appl. Opt. **37**(22), 5271–5283 (1998).
31. J. Trevino, S. F. Liew, H. Noh, H. Cao, and L. Dal Negro, "Geometrical structure, multifractal spectra and localized optical modes of aperiodic Vogel spirals," Opt. Express **20**(3), 3015–3033 (2012).
32. E. D. Palik, *Handbook of Optical Constants of Solids* (Academic Press, 1997).

1. Introduction

Introducing disorder in a periodic structure such as a thick grating or a photonic crystal can lead to specific behaviors, such as strong absorption [1–3], enhanced transmission [4–6], or controllable transport properties including localization [7–11]. In nature, partially ordered structures with different types of disorder commonly induce selective reflection of light [12], such as happens with iridescent or non-iridescent colors generated by partially ordered structures of bird feathers [13,14], or blue or purple sheen produced by partially ordered arrays of surface tubercles of beetles [15,16].

Anodizing of aluminum plates is known to generate a few micrometer thick alumina layer comprising cylindrical nanopores (300 nm diameter) extending essentially perpendicular to the substrate. The pore distribution over the surface exhibits a short-distance order close to an hexagonal arrangement, however long-distance order cannot be defined. Visual observation of such nanoporous layers shows bright specular reflected colors in the visible spectrum due to optical interference [17]. It was shown, for example, that nanoporous films processed by phosphoric acid show increased disorder, lower reflection, and higher color saturation compared to those processed by oxalic acid [18]. To modify the effective refractive index and

#228505 - $15.00 USD Received 24 Nov 2014; revised 19 Jan 2015; accepted 29 Jan 2015; published 12 Feb 2015

the optical thickness of the reflecting film and consequently modify the observed color, other materials can be associated to these nanoporous alumina layers. For instance, carbon nanotubes have been deposited onto a nanoporous alumina layer using chemical vapor deposition, resulting in more saturated colors [19]. The color of such composite layer has been further tuned by reducing the film thickness and increasing the pore diameter using chemical etching [20]. In another example, the color of Cr-coated nanoporous alumina film was tuned by controlling the pore depth [21]. One further color tuning method of multilayer interference is to fill nanoporous alumina film with TiO_2 [22].

Until now, the mechanism of such color effects observed for nanoporous alumina layers has been explained only in a crude way, namely, from the straightforward application of Bragg's equation with an effective refractive index [17–22]. This approach only gives an order of magnitude of the peak positions in the reflectance spectrum, but cannot predict the whole spectrum. Rigorous two-dimensional (2D) finite-difference time-domain calculations have been performed to simulate partially ordered nanoporous alumina films illuminated in guided light conditions, i.e. parallel to the layer. These simulations showed photonic stop bands of transmittance [23], but no results have been presented when the sample is illuminated under some arbitrary incidence. Homogenization (also called "effective medium") theories also do not account for those color effects.

In this article, we investigate the specular reflectance of a partially ordered nanoporous alumina film on an aluminum substrate by using the method of Rigorous Coupled Wave Analysis (RCWA [24–26]). Introduction of disorder, i.e. the deviations from periodicity in terms of nanopore location and nanopore radius, has driven this work. We focus on the reflectance spectrum in the specular direction, i.e. the specular value of the normalized bidirectional reflectance distribution function (BRDF). Because the computer resources required for a full 2D investigation exceeded our possibilities, a one-dimensional (1D) model mimicking the 2D samples has been devised. Although it cannot be expected to reproduce the 2D effects completely, the present work is an attempt to at least reproduce the main trends. A model material is built based on statistical dimensional characteristics determined by image analysis of Scanning Electron Microscopy (SEM) images of a nanoporous alumina layer obtained experimentally. The simulated specular reflectance spectrum is calculated and compared with the BRDF measured experimentally. Our aim here is to determine which statistical features have the largest impact on the material's optical properties. The longer term goal is to simulate the general trend of the optical response based on morphological parameters and so be able to produce samples with specific optical effects.

2. Sample preparation and characterization

2.1 Sample elaboration

Through the anodizing process, alumina is formed at the surface of aluminum alloys. As described in the literature [17–22,27], specific chemical processes may in particular form nanopores exhibiting a tubular structure that extends perpendicularly to the substrate throughout the alumina layer.

The sample we investigate in this work was obtained by electrochemical anodizing of 1 mm thick Aluminium-Magnesium alloy (Al 5754, 95% Al) plates with a custom-made anodizing cell. The anodizing area was 30 cm^2. Before anodizing, the aluminium plates were polished and etched 10 min in phosphoric acid to remove the native alumina layer. The anodizing process was performed in phosphoric acid (3×10^{-4} mol/L^{-1}) under vigorous stirring in a temperature controlled bath at 195 V. It might be appropriate to point out that since the process creates a nanoporous alumina layer, alumina layer without nanopores is not available as reference for comparison.

2.2 Morphological characterization

The morphology of the alumina layer has been characterized using SEM (ZEISS Ultra 55). Figure 1 shows a top view (1(a)) and a side view taken on a fracture of the alumina layer

#228505 - $15.00 USD Received 24 Nov 2014; revised 19 Jan 2015; accepted 29 Jan 2015; published 12 Feb 2015

(1(b)). The top view clearly shows a set of pores running perpendicular to the substrate, which are the main interest of this work. The side view reveals, in addition to those primary pores, another set of roughly tubular pores of slightly smaller diameter connecting the former ones and running perpendicularly to them. The first set of pores will be designated as "big nanopores" and the second as "small nanopores". From Fig. 1(a), the porosity of the big nanopores, is estimated to be $f_b = 0.32$ based on the surface fraction.

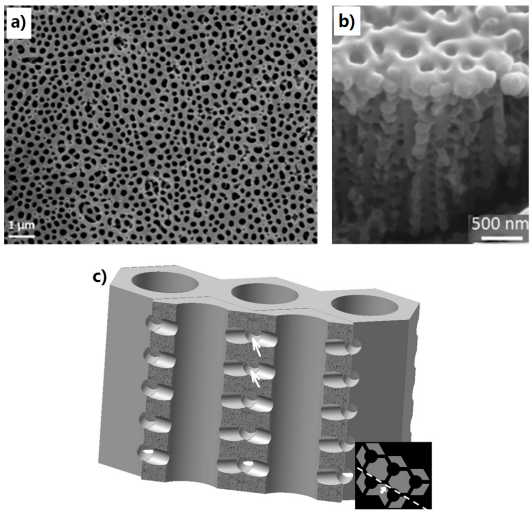

Fig. 1. (a) Top view of SEM measurement results of our fabricated partially ordered nanoporous alumina film on aluminum substrate, (b) side view of a fractured part of the same sample and (c) 3D-scheme of the porous morphology.

Although significant distortion is conspicuous, we can observe on Fig. 1(a) that the local arrangement of the big nanopores is approximately hexagonal. A model morphology of the porosity can be drawn on Fig. 1(c), where both types of porosity are shown. Figure 1(b) gives an estimation of both the diameter and the distance between two small nanopores, the porosity of the small nanopores is then roughly estimated geometrically around $f_s = 0.14$. The total porosity, defined as the volumetric fraction of air in the alumina layer, can be estimated as the sum of both porosities, and is thus equal to $f_p = 0.46$. The filling fraction is defined as $1 - f_p$.

The thickness of the alumina layer was evaluated through SEM observations on the cross section of the sample. The cross-section exhibits rough profiles for both the aluminum-alumina and alumina-air interfaces (also illustrated on Fig. 1(b)). The thickness is then evaluated around 2.6 μm.

To evaluate the average inter-big nanopore distance, we apply 2D Fast Fourier transform of the SEM images and obtain that each big nanopore counts six nearest neighbors. Figure 1(a) also hints at a hexagonal arrangement of the big nanopores although it is apparent only at some places. a_i is defined as the average distance between the center of one arbitrary big nanopore and the center of its six nearest neighbors. r_i is defined as the radius of one arbitrary big nanopore. a_i and r_i are both found to approximately follow normal distributions, as is further detailed in the doctoral dissertation by one of us [27]. The average spacing $\bar{a}$, calculated over the whole SEM image, between two neighboring big nanopores $\bar{a} = \dfrac{\sum_{i=1}^{N} a_i}{N}$ is found to be $\bar{a} = 334$ nm. The standard deviation of the spacing

#228505 - $15.00 USD Received 24 Nov 2014; revised 19 Jan 2015; accepted 29 Jan 2015; published 12 Feb 2015

$S_a = \sqrt{\frac{\sum_{i=1}^{N}(a_i - \bar{a})^2}{N-1}}$ is $S_a = 26.4$ nm. The average radius of the big nanopores $\bar{r} = \frac{\sum_{i=1}^{N} r_i}{N}$ is $\bar{r} = 101$ nm and the standard deviation $S_r = \sqrt{\frac{\sum_{i=1}^{N}(r_i - \bar{r})^2}{N-1}}$ is $S_r = 18.0$ nm.

2.3 Experimental specular reflectance spectrum

Optical measurements of the here studied sample have been carried out using a custom-made gonio-spectroreflectometer which some of us described elsewhere [28]. Throughout the present work we concentrate on the specular reflectance spectrum, which was measured with a detector solid angle (7.1×10^{-6} steradian) smaller than the source solid angle (1.3×10^{-5} steradian).

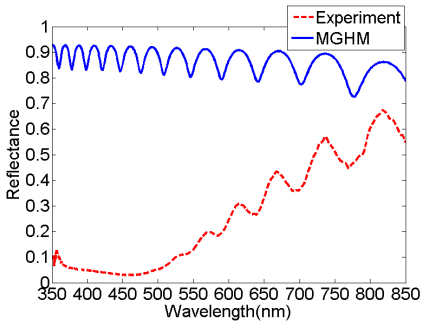

Fig. 2. Experimental specular reflectance of the here studied sample for an incidence angle equal to 45° (dashed red curve) and calculated specular reflectance considering the Maxwell-Garnett homogenization model (MGHM, solid blue curve) for porous alumina film.

Figure 2 shows the experimental specular reflectance of the studied sample for an incidence angle equal to 45° (dashed red curve). The reflectance increases gradually and smoothly from the blue region to the red region of the spectrum, where in addition several oscillations are visible. Our interest in this work concentrates on the general shape of this curve. The blue curve on Fig. 2 corresponds to the calculated specular reflectance considering a homogeneous non absorbing layer deposited on aluminum. The thin layer index was calculated here by applying the Maxwell-Garnett homogenization model [29] (further detailed below for another purpose) to porous alumina with porosity f_p. For the refractive index of aluminum, we use Lorentz-Drude model [30]. Similar oscillations appear and can clearly be attributed to a standard thin film interference effect. Adjusting the homogeneous medium index and thickness allows matching the maxima and minima with those of the experimental curve, but the general trend is quite different, as the average reflectance remains high in the blue region. However, the choice of the exact value for the refractive index plays little role: the meaningful conclusion at this point is that the general trend of the reflectance curve cannot simply be explained by using homogenization theory. In the following, we shall investigate whether diffraction effects by "disorder" in big nanopores can account for it. In particular, the role of dispersion in the big nanopores spacing and size will be evidenced.

3. Modeling, simulations and discussions

3.1 Modeling method

The experimental sample has a 2D distribution of nanopores while our calculation is 1D. However, to introduce the discussion, let us at first explain the principle of our modeling work without reference to dimensionality. We simulated the specular reflectance spectrum of

#228505 - $15.00 USD Received 24 Nov 2014; revised 19 Jan 2015; accepted 29 Jan 2015; published 12 Feb 2015

nanoporous alumina with RCWA. This method is based on Fourier series expansions of the permittivity and the electromagnetic fields inside the studied material.

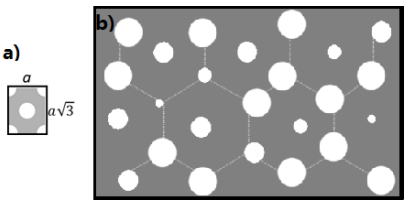

Fig. 3. (a) An elementary RCWA cell in the case of a perfectly hexagonal structure and (b) an elementary RCWA cell in the case of a disturbed structure. The small white dotted lines are guides for the eyes to show the displacing of the pores from the hexagonal structure.

Pair correlation statistics [31] would be a more direct but less complete way to account for the same distribution of big nanopores centers. We chose to model the real material by using one rigorous electromagnetic theory to fully account for the interactions between diffracted waves from the individual nanopores. To explain how the RCWA method is implemented here, Fig. 3(a) shows the non-disturbed unit cell for a periodic hexagonal structure. The RCWA cell that we use covers several such unit cells, with all nanopore radii and locations modified according to a normal distribution to simulate the disorder, as shown on Fig. 3(b). The calculation is repeated P times with different random realizations and averaged. In each of the P instances, the model material is therefore considered as a grating with a period much larger than the non-disturbed unit cell.

In our simulations, Fourier series expansions are limited to N_{harm} Fourier harmonics. In the numerical implementation, we start from N identical tubular nanopores, all with the same radius r, into a periodic lattice with the same spacing a, in a nanoporous alumina layer with a thickness t. Next, we move the central locations of the pores randomly with a normal distribution of standard deviation σ_{cl} and change their radii randomly with a normal distribution of standard deviation σ_r, nevertheless preventing the nanopores from overlapping. The sample is assumed to be illuminated with collimated light coming from above the nanoporous alumina layer at an incidence angle of $\theta = 45°$, as in the experimental results that we seek to numerically simulate. As mentioned above, for each value of the parameters σ_{cl}, σ_r and t, we calculate P independent randomly generated model materials and then average them. To mimic non-polarized light, the results shown are an incoherent superposition of TE and TM excitation.

To keep the computational load manageable, our calculations are restricted to a fixed number N of big nanopores in the nanoporous alumina film. The small nanopores and alumina material together are just considered as a homogeneous medium with an equivalent refractive index n_{eqv} derived from the Maxwell-Garnett model [29]:

$$\frac{n_{eqv}^2 - n_{Al2O3}^2}{n_{eqv}^2 + 2n_{Al2O3}^2} = f_s' \frac{n_{air}^2 - n_{Al2O3}^2}{n_{air}^2 + 2n_{Al2O3}^2}. \quad (1)$$

where n_{air}, the refractive index of air, is assumed to be $n_{air} = 1$, and $n_{Al_2O_3}$, the refractive index of alumina, is assumed to be $n_{Al_2O_3} = 1.76$ [32], an average value used throughout the visible domain because alumina dispersion was found to play little role here. In Eq. (1), $f_s' = \frac{f_s}{1 - f_b}$ is the porosity of the alumina layer when the big nanopores are excluded. Therefore, the filling fraction of the effective medium excluding the big nanopores is $1 - f_s'$.

#228505 - $15.00 USD Received 24 Nov 2014; revised 19 Jan 2015; accepted 29 Jan 2015; published 12 Feb 2015

This leads to $n_{eqv} = 1.61$ for the effective refractive index of alumina with the small nanopores (with $f_s = 0.14$). For the refractive index of aluminum n_{Al}, we use Lorentz-Drude model [30].

To reach appropriate conclusions in a reasonable time considering the computing resources available, we had to perform the simulations on a 1D model. As measurements were taken on real, and therefore 2D samples, we conducted numerical simulations in 2D, but only on a fairly limited number of cases and with low values of N_{harm} and P, resulting in limited accuracy and reliability. It is therefore essential to properly design a 1D model that will most closely, if definitely not exactly, mimic the 2D effects. Those 1D simulations are the main subject of this work. In the following, although 1D depletions are in fact "grooves" rather than "pores", we keep the term "nanopore" by analogy with the real samples that we are simulating. For the 1D version we selected the average spacing between two nanopores to be identical to the 2D value. Systematically denoting with primed symbols the 1D quantities, that is expressed as $a' = a = \overline{a} = 334$ nm. We selected the nanopore average radius in such a way as to keep the volume fraction of big nanopores equal to $f_b = 0.32$, which leads to $r' = \frac{a' \cdot f_b}{2} = 53.3$ nm.

Sections S1, S2, and S3 of the supplement show how the values for N and P, together with the number of harmonics in the Fourier series expansion were selected. In section S4 we also show, on one fairly simple case, that a 1D simulation reproduces the 2D simulation relatively well. Further discussion about the statistical distributions used in 1D compared to the 2D experimental evidence is provided in section S5. The thickness of the nanoporous alumina film is taken equal to $t = 2538$ nm. The choice of this value is explained in section S6.

3.2 Dispersion in the nanopore central location

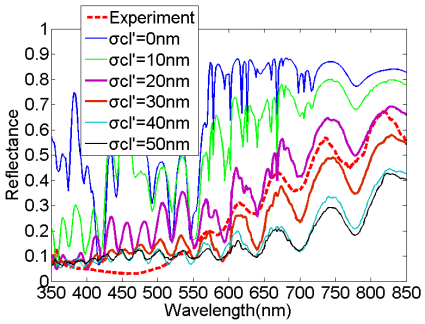

Fig. 4. (All solid curves) Simulated reflectance spectra for a RCWA elementary cell consisting of $N = 25$ nanopores, with the standard deviation $\sigma_{cl'}$ increasing from 0 nm to 50 nm in steps of 10 nm. Each spectrum is calculated for $P = 30$ random drawings of the elementary cell, for TE and TM polarizations and with a number of Fourier harmonics $N_{harm} = 4N$ respectively, and finally averaged. The dotted red curve corresponds to the experimental data.

We generated a model material with an RCWA elementary cell consisting of $N = 25$ alumina nanopores, with a random displacement of the central location of the nanopores following a normal distribution of standard deviation $\sigma_{cl'}$. $\sigma_{cl'}$ was increased from 0 nm to 50 nm in steps of 10 nm. The resulting averaged reflectance spectra are shown on Fig. 4 over the wavelength range [350 nm, 850 nm]. In this and all subsequent simulations, the wavelength was sampled by steps of 2 nm. The amplitude and the oscillation of the reflectance spectrum decrease greatly when the standard deviation increases from 0 nm to 30 nm, approaching the experimental curve. Then the amplitude tends to saturate and the oscillation decreases in the

#228505 - $15.00 USD Received 24 Nov 2014; revised 19 Jan 2015; accepted 29 Jan 2015; published 12 Feb 2015

blue region, while in the red region the amplitude and the oscillation keep decreasing when the standard deviation changes from 30 nm to 50 nm.

Disorder in the spacing between nanopores gives the proper behavior in the red region of the spectrum. Although it does not give satisfactory results in the blue region, these curves nevertheless clearly suggest that disorder in the big nanopores spacing plays a central role in the behavior of these structures, which cannot be explained just by homogenization techniques. Nevertheless, that is not enough for a good fit and the variance in the radius may play a role.

3.3 Dispersion in the radius value

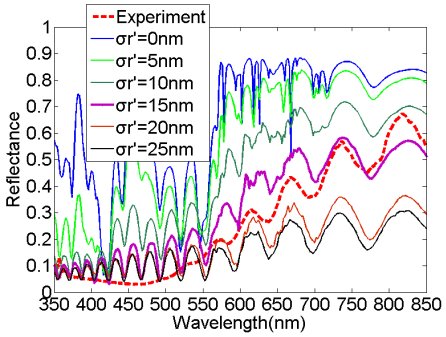

Fig. 5. (All solid curves) Simulated reflectance spectra for a RCWA elementary cell consisting of $N = 25$ nanopores, with the standard deviation $\sigma_{r'}$ of the nanopores radius increasing from 0 nm to 25 nm in steps of 5 nm. Each spectrum is calculated for $P = 30$ random drawings of the elementary cell, for TE and TM polarizations and with a number of Fourier harmonics $N_{\text{harm}} = 4N$ respectively, and finally averaged. The dotted red curve corresponds to the experimental data.

Here, we fixed the alumina nanopores center on the periodic lattice and generated model materials with an elementary cell consisting of $N = 25$ alumina nanopores, with a random variation of the radius size following a normal distribution with a standard deviation $\sigma_{r'}$. $\sigma_{r'}$ was increased from 0 nm to 25 nm in steps of 5 nm. The resulting reflectance spectra are shown on Fig. 5. The amplitude and the oscillation of the reflectance decrease gradually when the radius variation amplitude changes from 0 nm to 15 nm. Similarly, the amplitude and modulation saturate in the blue region while they keep decreasing in the red region.

The main differences between the present simulation and the previous one presented in Section 3.2 are stronger oscillations in the blue region in the present case and a saturation of the average reflectance (aside from the thin film interference oscillations) in the red region. For a better fit of the experimental reflectance, we should combine random fluctuations in both the central location of the nanopores and their radius. Rather than trying an optimization, our approach was to select the values of the standard deviation of those two random parameters from observations of SEM images of our sample.

#228505 - $15.00 USD Received 24 Nov 2014; revised 19 Jan 2015; accepted 29 Jan 2015; published 12 Feb 2015

3.4 Fitting the simulation parameters with morphological parameters of the real material

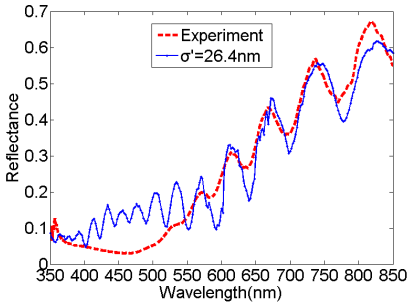

Fig. 6. (Blue solid curve) Simulated reflectance spectrum for an elementary cell consisting of N = 25 nanopores, with a standard deviation σ' = 26.4 nm corresponding to the standard deviation of the left and right side walls of the alumina nanopores. Each spectrum is calculated for P = 30 random drawings of the RCWA elementary cell, for TE and TM polarizations and with a number of Fourier harmonics $N_{harm} = 4N$ respectively, and finally averaged. The dotted red curve corresponds to the experimental data.

In order to best correlate 1D model parameters and those extracted from 2D SEM image observations, we combined the values of the standard deviation of the central pore location $\sigma_{cl'}$ and this of the radius $\sigma_{r'}$. As explained in section S5 of the supplement, the best result is a combined standard deviation $\sigma' = \sqrt{\sigma_{cl'}^2 + \sigma_{r'}^2} = 26.4$ nm, corresponding to the standard deviation of the left and right side walls of the alumina nanopores. The calculated reflectance curve is shown on Fig. 6 together with the experimental result. The simulated curve provides a relatively good fit of the experimental result in the red region from 550nm to 850nm. In the blue region, there are oscillations on the simulated curve, but there is no oscillation on the experimental curve and the amplitude of the simulated reflectance is larger than that of the experimental result. This issue will be considered below.

3.5 Discussion about the blue region (λ = 350-500 nm)

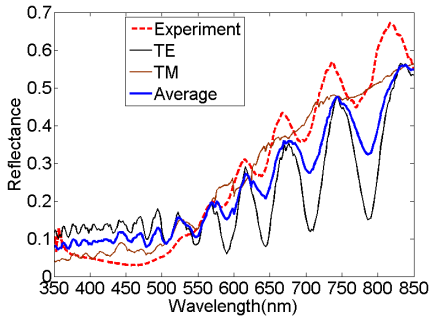

Fig. 7. (All solid curves) Simulated reflectance spectra for an elementary cell consisting of N = 25 big nanopores with a standard deviation σ' = 26.4 nm corresponding to the standard deviation of the left and right side walls of the alumina nanopores. We also introduced in the model small nanopores with a radius $r_{s'}$ = 22.7nm between each pair of neighboring big nanopores. Each spectrum is calculated for P = 30 random drawings of the RCWA elementary cell, for TE (black curve) and TM (brown curve) polarizations and with a number of Fourier harmonics $N_{harm} = 4N$ respectively, and finally averaged over the random drawings. The blue curve corresponds to the additional average over polarization. The dotted red curve corresponds to the experimental data.

To address the issue of the discrepancy between experimental data and our previous simulations in the blue region, we investigated the role of the small nanopores. We inserted

#228505 - $15.00 USD Received 24 Nov 2014; revised 19 Jan 2015; accepted 29 Jan 2015; published 12 Feb 2015

one small nanopore with the radius $r_s' = \frac{f_s \cdot a'}{2} = 22.7$ nm between each pair of neighboring big nanopores and parallel to them. This crude description would only account for the presence of small nanopores but not for the orientation. Big nanopores description is kept with the same statistical parameters as that of Fig. 6. The reflectance spectrum of this kind of alumina nanopores layer has been calculated and shown together with the experimental result on Fig. 7. By introducing small nanopores into the simulation model, we can see that the oscillations of the reflectance are reduced in the blue region while the amplitude of the reflectance in the red region also decreases because the small nanopores scatter more incident energy, especially in the blue region. This indicates that a more sophisticated model for small nanopores together with a revision of the parameter set developed above could lead to improved results. In that model, the existence of small nanopores with various orientations, including parallel to the substrate, should be taken into account.

On Fig. 7, the difference between TE and TM polarizations is also shown. The TM reflectance curve is seen to drop to lower values in the blue region and to show damped oscillations.

4. Conclusions

We have modeled the reflectance of a partially ordered nanoporous alumina layer on aluminum substrate by using RCWA method and by considering normally distributed variations of the central locations and radius sizes of the alumina nanopores. Our 1D model is in accordance with the fact that such samples exhibit relatively saturated reddish – orange colors in the specular direction. While the oscillations in the reflectance spectrum corresponding to thin film interferences between the alumina layer top and bottom interfaces were well reproduced by numerically adjusting the thickness value in our model, no such optimization was necessary to reproduce the general trend of the reflectance function, which, starting from the red end of the spectrum, progressively decreases to end up with fairly low values in the blue region. Instead, the statistical average and standard deviation of big nanopores radius and location derived from SEM images observations were appropriate to reproduce that trend. Of course, we cannot claim that no other explanation is possible but we can say that the model of disorder that we simulated does reproduce the main trends observed experimentally.

Future work on this subject should address the most conspicuous departure of our simulation results from experimental ones, which at this stage is the fact that the reflectance in the blue region is fairly low and does not show any oscillation, while our model predicts a small but nevertheless higher value, and shows interference oscillations. We expose here below four directions that should be explored to solve that remaining discrepancy and will deserve further investigation:

i) The low value in the blue could be a strictly 2D effect with no 1D equivalent. In particular, the difference between TE and TM polarization may well be different in 1D compared to 2D.

ii) Another possibility is that larger RCWA elementary cells are required for a good fit in the blue region. Section S3 in the supplement tends to suggest that the issue is worth exploring.

iii) The bottom of the alumina surface at the aluminum interface is rough, as can be easily observed experimentally with a SEM. That roughness is likely to scatter blue wavelengths more than red ones. Further 1D simulations could address that issue.

iv) Most probably, taking into account small nanopores in a more complete way than in Section 3.5, while fairly heavy from a computational point of view, is a promising approach.

#228505 - $15.00 USD Received 24 Nov 2014; revised 19 Jan 2015; accepted 29 Jan 2015; published 12 Feb 2015

Acknowledgments

Calculations used the RETICOLO software written by Ph. Lalanne and J.P. Hugonin [26]. In this case, RETICOLO was used in the RCWA mode for modelling diffraction by 1D gratings. No perfectly matched layer was used to limit the size of the cell. We thank Ph. Lalanne as well as the anonymous reviewers for useful suggestions. Dengfeng Kuang acknowledges the financial supports provided by the China Scholarship Council (CSC) as a visiting scholar (File No. 201208120076) and the National Natural Science Foundation of China (NSFC), grant 11274186.

#228505 - $15.00 USD Received 24 Nov 2014; revised 19 Jan 2015; accepted 29 Jan 2015; published 12 Feb 2015